THE JOURNAL OF PHYSICAL CHEMISTRY C

Article

pubs.acs.org/JPCC

Reduced Graphene Oxide/Fe_3O_4/Polyaniline Nanostructures as Electrode Materials for an All-Solid-State Hybrid Supercapacitor

Sanjoy Mondal, Utpal Rana, and Sudip Malik*

Polymer Science Unit, Indian Association for the Cultivation of Science, 2A & 2B Raja S. C. Mullick Road, Jadavpur, Kolkata − 700032, India

Supporting Information

ABSTRACT: We have synthesized a ternary rGO/Fe_3O_4/PANI (rGFP) composite for binder-free, semiflexible, thin, all-solid-state supercapacitor device fabrication. A scalable soft-template technique has been adopted for the preparation of three-dimensional Fe_3O_4-decorated reduced graphene oxide (rGO)-doped polyaniline (PANI) nanorods that are unambiguously investigated under electron microscopes (FESEM and HRTEM). The presence of PANI in the nanocomposite is overwhelmingly supported by the absorption and vibration studies. Raman spectra convincingly show the presence of rGO in the nanocomposites, and the formation of Fe_3O_4 nanoparticles is confirmed by XRD and XPS results. The specific capacitance value that has been achieved for synthesized ternary rGFP nanocomposite is ∼283.4 F/g at 1.0 A/g current density and exhibited a maximum energy density of 47.7 W h/kg at a power density of 550 W/kg. Interestingly, after 5000 cycles the composite shows excellent life stability that is a 78% retention of the electrochemical property. To demonstrate the portable energy storage applicability, a binder-free rGFP-based supercapacitor device was fabricated, which illustrated the operation of an LED bulb for 30 min when fully charged. These results indicate that synthesized ternary nanocomposites are worth their potential as an electrode material and would be used in next-generation high-rate energy storage systems.

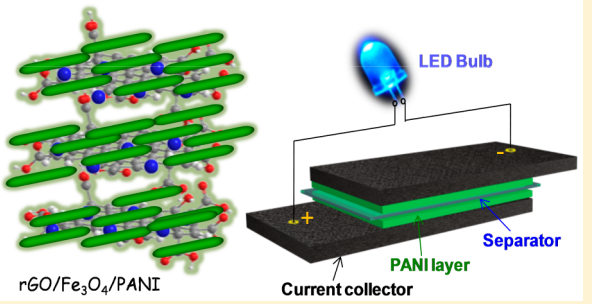

INTRODUCTION

The design and development of sustainable, low-cost, renewable, and high-performance energy storage devices have important issues owing to the tremendous need for energy consumption at every step in our modern daily lives.[1−3] Among the different energy storage devices, supercapacitors or electrochemical capacitors are very promising in terms of their portability, high efficiency, fast charge−discharge capability, long lifecycle stability, operational safety, and high power density,[4−6] with many advantages over batteries.[7−9] Different kinds of materials such as metal oxides,[10,11] carbon (CNTs/graphene),[12,13] composites,[14] and polymers[15,16] have been used to make both symmetric and asymmetric supercapacitor devices. A supercapacitor is generally operated by electrolytes, and the choice of electrolyte is one of the important factors for energy storage performance. Generally, conventional energy storage devices are operated by a liquid electrolyte; however, the safety issue limited their importance. Therefore, the replacement of liquid electrolyte by a solid electrolyte or separator is necessary for the development of lightweight, safe,[17−19] flexible, thin energy storage devices.[20,21] Importantly, a solid electrolyte supercapacitor effectively avoids the short-circuit problem, caused by the leakage of electrolyte, diminishes the mass loss of active materials, increases the mechanical strength of devices, and many others. Additionally, packaging or additive material is not necessary, and there is an effortless postprocess for device fabrication. Finally, thin all-solid-state supercapacitors integrated with a microsensor and microelectronic devices are easily utilized as a dominant power source.[22,23]

Recently, ternary composites have been used as enhance supercapacitor materials, namely, carbonaceous materials, transition-metal oxides, and conducting polymers.[10−16] In the case of carbonaceous material, graphene is well known because of its unique electrical, mechanical, and chemical properties with a high specific surface area.[7,19,21] Among all of the metal oxides/hydroxides, Fe_3O_4 is one of the attractive materials used for pseudocapacitor materials because its considerably large operational potential window range (−1.2 to 0.25), high theoretical capacitance value (2299 F/g), natural abundance, low cost, and low toxicity make it suitable for use as an electrode material.[21,22] Additionally, in cyclic voltammetry, single redox behavior contributing a pseudocapacitor property to the composite material makes it a hybrid capacitor. The nanostructure of a ternary composite by the combination of PANI with graphene oxide and transition-metal oxides should be an effective material for improving the stability and energy storage capacity of a solid-state electrode. Although different

Received: November 1, 2016
Revised: February 27, 2017
Published: February 27, 2017

DOI: 10.1021/acs.jpcc.6b10978
J. Phys. Chem. C 2017, 121, 7573−7583

Scheme 1. Schematic Presentation for the rGO/Fe_3O_4 (rGF) and rGO/Fe_3O_4/PANI (rGFP) Composite Preparation

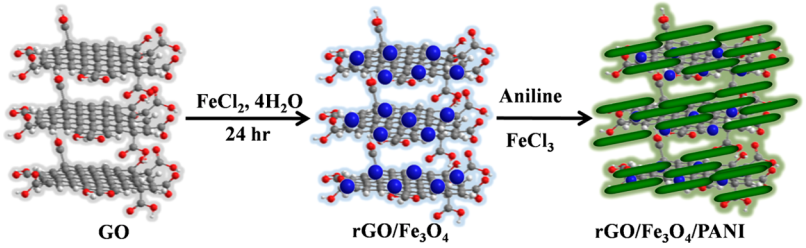

ternary composites as electrode materials for electrochemical capacitors are well known in the literature, the demonstration of the solid-state binder-free device, which significantly restricts their practical applications in supercapacitors, is rare. Again in the conducting polymer families, polyaniline (PANI) is very popular because of its easy synthesis, low production cost, high thermal or environmental stability, high-range electrical conductivity, and so on.[16,24−26] Moreover, PANI can store charges in the electrical double layer as well as by the Faradaic charge-transfer mechanism. Hence, combining PANI with graphene-based materials can increase the specific capacitance of the composites. Apart from these nanostructures of PANI, nanotubes have received more attention in the electrochemical capacitor because of the high specific area of the electrode with the slower diffusion path of the electrolyte.[27,28] Our group has successively developed a simple synthesis technique for polyaniline nanotubes with size and shape control using graphene oxide.[24] Our most recent study demonstrated that graphene quantum dot-doped polyaniline nanotubes have greatly improved the specific capacitance of the composite.[16]

Here, we have reported the synthesis of ternary nanostructure materials for the fabrication of a high-energy-density binder-free all-solid-state supercapacitor device. A facile, scalable soft-template-based method has been developed to make the ternary nanostructure. The synthesized ternary rGO/Fe_3O_4/PANI (rGFP) composite shows nanorod-like morphology, which has been directly used as the electrode material for fabricating the binder-free solid-state hybrid supercapacitor devices. The rGFP ternary composites have showed a relatively high capacitance of ∼283.4 F/g at 1.0 A/g current density in a solid-state two-electrode system, rather than rGF and GO only. The ternary rGFP composites have also exhibited a maximum energy density of 47.7 W h/kg at a power density of 550 W/kg with good lifecycle stability that includes a 78% retention of the electrochemical property after 5000 cycles. Furthermore, an rGFP-based supercapacitor device has been fabricated to demonstrate the practical application of the materials by LED illumination for up to 30 min.

EXPERIMENTAL SECTION

Materials. Powdered graphite (12 500, 500 mesh), poly(vinyl alcohol) (PVA), iron(II) chloride tetrahydrate ($FeCl_2·4H_2O$), and iron(III) chloride ($FeCl_3$) were purchased from Sigma-Aldrich and used in the experiment without further purification. Aniline (distilled under reduced pressure and stored at 5 °C in the dark prior to use), hydrogen peroxide (H_2O_2, 30% v/v), potassium permanganate ($KMnO_4$), sodium nitrate ($NaNO_3$), sulfuric acid (H_2SO_4, 98%), and phosphoric acid (H_3PO_4, 85%) were supplied by Merck Chemicals. LED bulbs (∼1.5 V) were purchased from the local market. All solutions were made in and all reactions were carried out in water (18 MΩ cm, Millipore Milli-Q water system).

Characterization and Instrumentation. The surface morphology of synthesized GO, rGO/Fe_3O_4 (rGF), and rGO/Fe_3O_4/PANI (rGFP) composites was characterized by an FESEM (JEOL, JSM 6700F) instrument operating at 5 kV. TEM imaging of all composites was carried out on an HRTEM (JEOL, 2010EX) instrument at an accelerating voltage of 200 kV. UV−vis spectroscopy was performed with an Agilent (model 8453) UV−vis spectrophotometer. FTIR spectroscopy was carried out with an FTIR-8400S instrument (Shimadzu) using KBr pellets. Powered XRD analysis was performed with a Bruker AXS diffractometer (D8 advance) using Cu Kα radiation (λ = 1.54 Å), a generator voltage of 40 kV, and a current of 40 mA. Thermogravimetric analyses (TGA) were done with a TA thermal analysis system from 25 to 550 °C with a heating rate of 10 °C/min under an N_2 atmosphere. An XPS experiment on a synthesized rGFP composite was performed by using a focused monochromatized A1 Kα X-ray source (1486.8 eV) in an Omicron Nano-Technology 0571 XPS instrument. A Raman study was carried out with a Raman spectrometer (model T-64000, Horiba-Jobin Yvon) excited with a 514.5 nm laser. All electrochemical experiments such as cyclic voltammetry (CV), galvanostatic charge/discharge (GCD), and electrochemical impedance spectroscopy (EIS) were carried out using a CHI6087E electrochemical workstation (CHI, USA) with a two-electrode system as well as a three-electrode system. CV and GCD studies were carried out over the potential range of −0.2 to 0.9 V, and EIS studies were performed in the 0.1 Hz to 100 kHz frequency range.

Preparation of the rGO/Fe_3O_4 (rGF) Composite. Synthesized GO (10 mg) was dispersed in 10 mL of water by sonication to make a well-distributed GO solution. $FeCl_2·4H_2O$ (100 mg) was added to a dispersed solution of GO with a 1:10 w/w ratio of GO to $FeCl_2·4H_2O$ at room temperature (25 °C) with vigorous stirring for 12 h. A color change of the reaction from yellow to dark black was observed. Synthesized rGF was washed several times with water by centrifugation. Finally, the product was purified by a dialysis membrane (M_w = 10 000) for 24 h and dried overnight in vacuum at 60 °C.

Preparation of the rGO/Fe_3O_4/PANI (rGFP) Composite. The rGFP composite was prepared according to Scheme 1. A presynthesized rGF composite was dispersed in water (1.0 mg/mL) with vigorous stirring. Aniline (1.0 mmol) was added to the rGF suspension with continuous stirring for 8 h at 25 °C. An aqueous $FeCl_3$ (5.0 mL, 1.0 mmol) solution was added dropwise to the resulting mixture with stirring at the same temperature for 30 min. The homogeneous reaction mixture was kept at 0−5 °C for 24 h with mechanical stirring. Finally, the green precipitate was washed with water and methanol several times and dried under vacuum at 60 °C to get greenish-black rGFP in powdered form.

PVA-H_3PO_4 Gel Electrolyte Preparation. The PVA-H_3PO_4 gel was prepared according to a reported procedure

DOI: 10.1021/acs.jpcc.6b10978
J. Phys. Chem. C 2017, 121, 7573−7583

Scheme 2. Schematic Presentation of Device Fabrication with Synthesized Ternary Composites

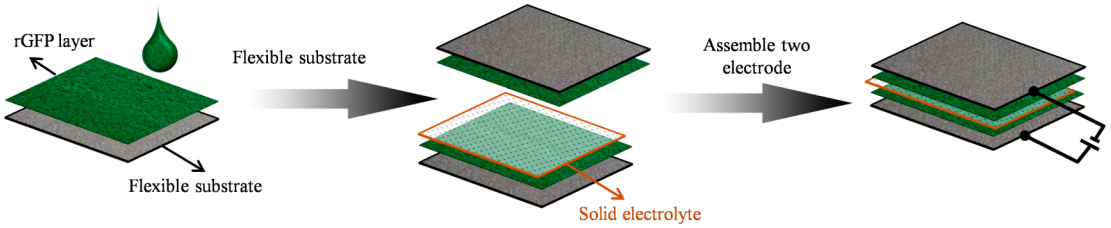

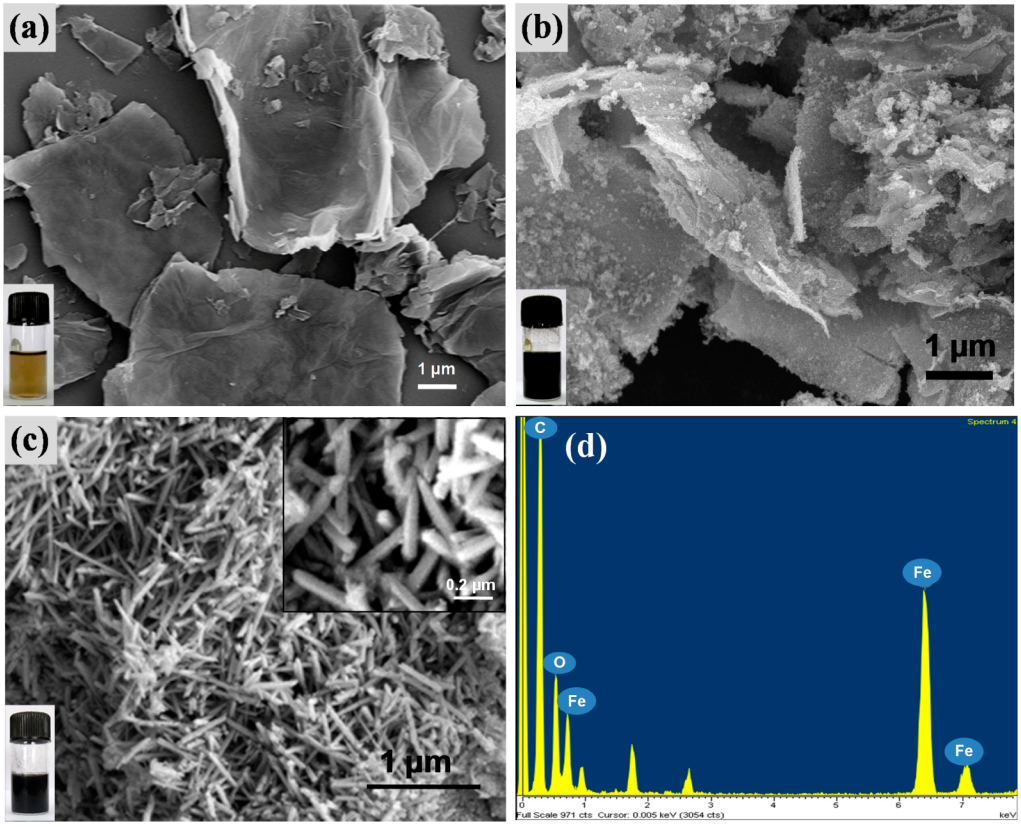

Figure 1. FESEM morphology with a digital bottle image (inset) of synthesized (a) GO, (b) rGF, (c) rGFP, and (d) EDX patterns for the rGFP composite.

with some modifcation.[29,30] Typically, 1.0 g of PVA pellets was dissolved in 10 mL of water at 90 °C under constant stirring until the solution became clear. After the solution was cooled to 25 °C, 1 mL of 85% concentrated H_3PO_4 was added, and slow stirring was continued until a clear solution was obtained. Later on, a synthesized PVA-H_3PO_4 gel was used as a solid electrolyte for device preparation.

Electrode Preparation and All-Solid-State Supercapacitor Device Fabrication. First, a paste of an rGFP composite was prepared in *N*-methyl-2-pyrrolidone (NMP) solvent with constant stirring at 25 °C for 2 h. A prepared rGFP paste was deposited over a 1.5 × 2.5 cm^2 electrode surface area. The uncoated part of the electrodes was used to connect devices in series. After being coated, the electrodes were dried in 60 °C under vacuum overnight. To make an all-solid-state supercapacitor device, two prepared electrode were sandwiched with the PVA-H_3PO_4 gel electrolyte and dried at 60 °C (Scheme 2). Three supercapacitor devices were connected in series to complete the cell that produced a working potential of ~3.0 V and a glowing LED bulb (~1.5 V) for up to 30 min.

The specific capacitance (C_s in F/g), energy density (E in W h/kg), and power density (P in W/kg) were calculated from the GCD curve based on eqs 1−3, respectively.[16,30]

$$C_s = \frac{i \times \Delta t}{\Delta V \times m} \text{ (F/g)} \quad (1)$$

$$E = \frac{1}{2} \times \Delta V^2 \times C_s \text{ (W h/kg)} \quad (2)$$

$$P = \frac{E}{\Delta t} \text{ (W/kg)} \quad (3)$$

where i is the current (A), Δt is the discharge time (s), ΔV represents the voltage windows (V), and m is the mass of the materials (g).

A conventional three-electrode technique, a modified glassy carbon electrode (GCE) as the working electrode, a saturated calomel electrode (SCE) as the reference electrode, a Pt wire electrode as the counter electrode, and 0.5 M H_3PO_4 as a liquid electrolyte were used. Prior to use, the GCEs (3 mm in diameter, surface area of 0.07 cm^2) were carefully polished with

DOI: 10.1021/acs.jpcc.6b10978
J. Phys. Chem. C 2017, 121, 7573−7583

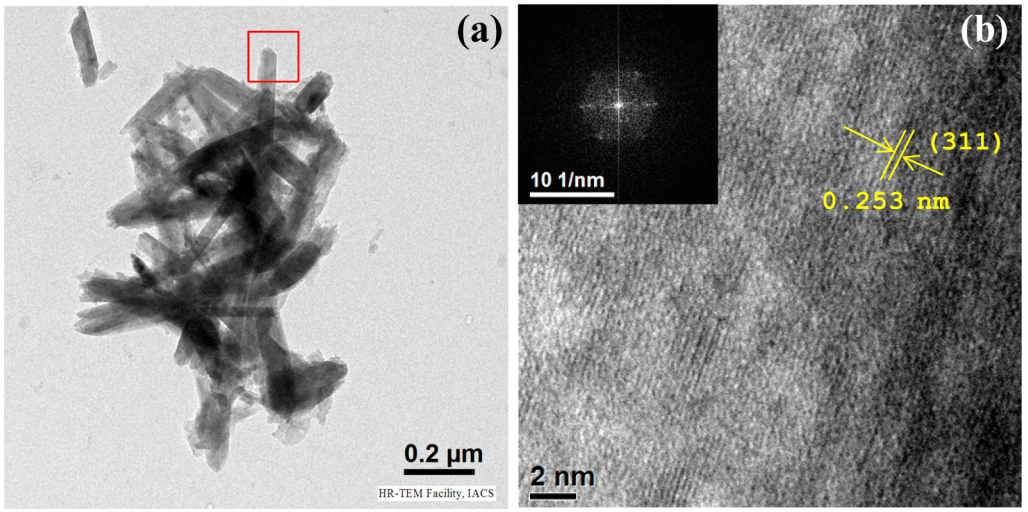

Figure 2. (a) TEM image of rGFP and (b) high -resolution image (inset image for SAED-patterned Fe_3O_4 NPs).

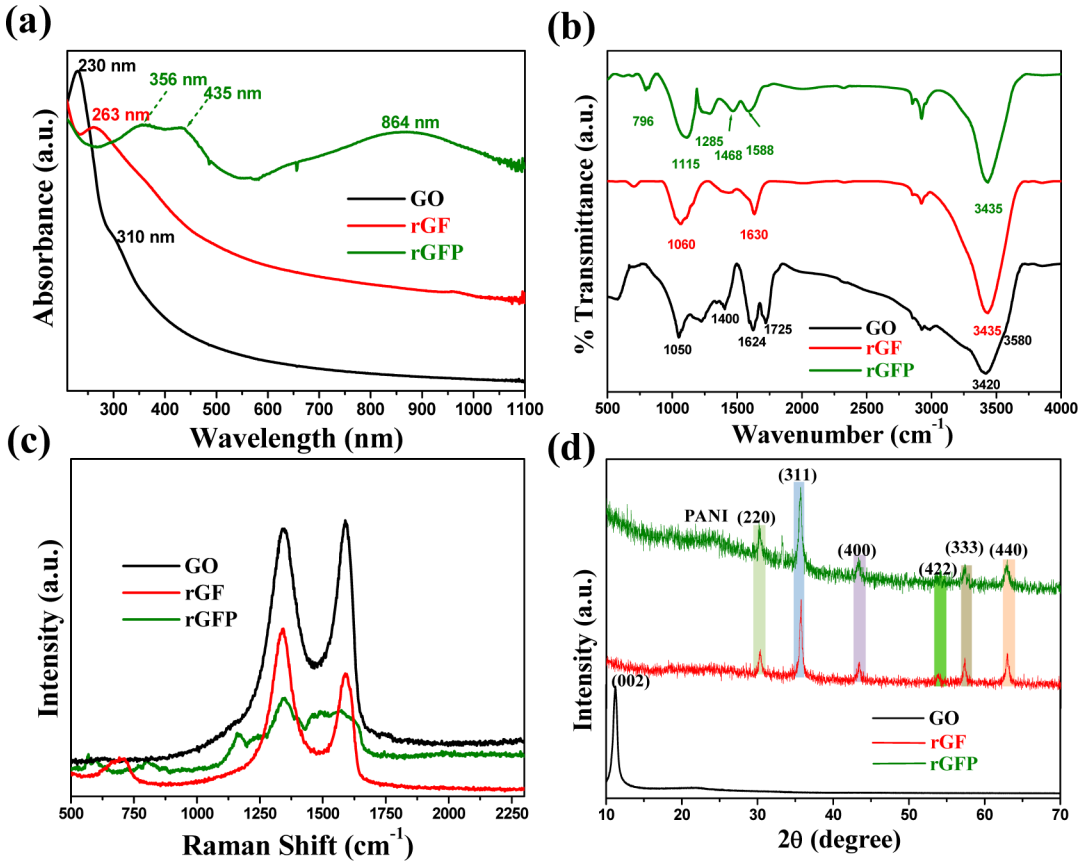

Figure 3. (a) UV–vis spectra of a water-dispersed solution. (b) FTIR spectra through a KBr pellet. (c) Raman spectra and (d) XRD pattern for synthesized GO (black line), rGF (red line), and rGFP (green line).

1, 0.3, and 0.05 μm alumina powder and sequentially washed with water and ethanol at room temperature until a mirror finish was obtained.

RESULTS AND DISCUSSION

Morphological Study. In this report, we demonstrate a novel and simple route to the synthesis of PANI nanorods doped with rGO-Fe_3O_4 nanostructures (Figure 1). The 2D sheetlike morphology of GO is shown in Figure 1a. Upon treatment of GO with $FeCl_2{\cdot}4H_2O$, the tiny Fe_3O_4-NPs are used to decorate GO sheets (Figure 1b). In the final step, aniline is oxidized to form PANI nanorod-like morphology in the presence of $FeCl_3$ as a mild oxidizing agent (Figure 1c). In the high-magnification SEM (Figure 1c, inset), it is found that all of the nanorods are quite uniform in shape with ~100 nm diameter and ~1–2 μm length. The EDX pattern of rGFP confirms that the composite has a high content of Fe (Figure 1d).

The nanorod-like morphology of the rGFP composite has been further confirmed by the TEM image shown in Figure 2a.

DOI: 10.1021/acs.jpcc.6b10978
J. Phys. Chem. C 2017, 121, 7573–7583

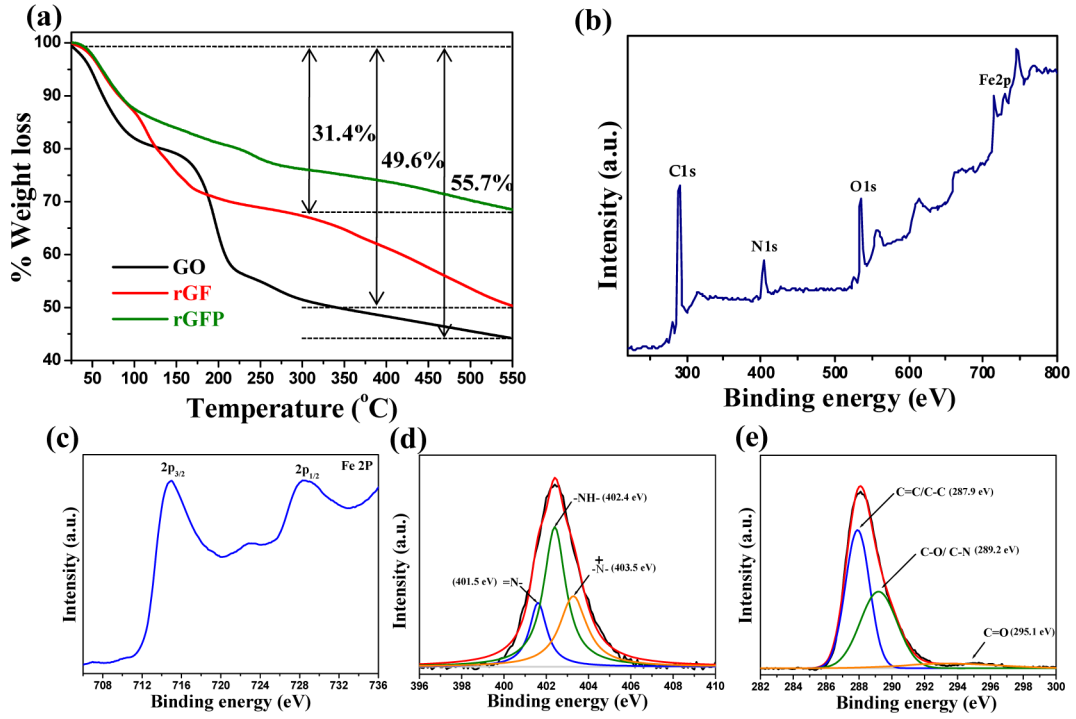

Figure 4. (a) TGA study under an N_2 atmosphere for synthesized GO (black line), rGF (red line), and rGFP (green line). XPS survey spectra of the ternary rGFP composite: (b) wide scan, (c) enlarged spectra of Fe2P, (d) N 1s, and (e) C 1s.

It is a surprising result as compared to our previous report, where GO-doped PANI formed good aspect ratio nanotube-like morphology.[24] The in-situ-synthesized spherically shaped Fe_3O_4 nanoparticles are quite homogeneously distributed on the PANI nanorod. Particles are not seen clearly because they are covered with PANI. The very careful observation of the Figure 2b fringe was present with a layer-to-layer distance of ~0.25 nm that exactly matches the (311) plane of the Fe_3O_4 nanoparticle in the XRD study and SAED pattern (inset image of Figure 2b).[31]

UV−Vis, FTIR, Raman, and XRD Study. The UV−vis spectra of water-dispersed GO, rGF, and rGFP composites are shown in Figure 3a. The GO have two distinct absorption peaks at ~230 nm corresponding to the $\pi-\pi^*$ transition of the aromatic C−C bond and a broad shoulder at 310 nm ascribed to the n−π^* transition of C═O bonds.[24,32,33] The absorption peak at 230 nm ($\pi-\pi^*$ transition of the aromatic C−C bond) for GO is shifted to 263 nm in rGF. This red shifting of ~33 nm occurs because of the increase in the conjugation length, revealing the reduction of graphene oxide (GO) to reduced graphene oxide (rGO).[34,35] In the rGFP composite, these peaks are not detectable owing to the large background of PANI. As the peaks for GO and rGO disappear concurrently, three characteristic absorbance peaks for PANI emerge at ~356, 435, and 864 nm, respectively. The absorption peak at ~356 nm is ascribed to the $\pi-\pi^*$ transition of benzenoid rings and that at 435 nm is ascribed to the polaron−π^* transition, and a dominant peak at ~864 nm represents the π−polaron transition of PANI chains.[24−26,36] Therefore, the absorption results clearly suggest the formation of PANI using $FeCl_3$ as an oxidizing agent and the simultaneous in situ reduction of GO to rGO.

To prove the formation of GO and rGO-doped PANI in the composites, FTIR studies of composites were performed (Figure 3b). The stretching vibrational band (black line in Figure 3b) at 1725 cm^{-1} for γC═O of the −COOH group, 1623 cm^{-1} for epoxide groups, and 1400 cm^{-1} for skeletal ring vibrations as well as tertiary C−OH groups present at the edge of the GO sheet and a broad band at 3460−3600 cm^{-1} for γO−H proved GO formation.[24,37] Again, after polymerization, the appearance of stretching bands at ~3430, 1588, 1468, 1285, 1115, and 796 cm^{-1} reveal the formation of PANI in the composite. The characteristic stretching vibrations at 3430 cm^{-1} for γN−H, 1588 cm^{-1} for γC═C of quinoid rings, 1468 cm^{-1} for γC═C of benzenoid rings, 1284 cm^{-1} for γC−N for the secondary aromatic amine, and 1102 and 796 cm^{-1} for the C−H aromatic in-plane and out-of-plane deformation for the 1,4-disubsituted benzene support the formation of PANI.[24−26]

In the Raman spectra (Figure 3c), GO, rGF, and rGFP have a couple of Raman-active bands, with the D band at 1345 cm^{-1} and the G band at 1595 cm^{-1} corresponding to defects or the edge and the vibration of sp^2-hybridized carbon, respectively. Raman spectra show that an increase in the D/G ratio, from ~0.96 for GO to ~1.34 for rGF to 1.12 for rGFP, indicates the formation of rGO during rGF and rGFP composite synthesis.[24] Apart from the D/G band ratio, two new peaks at 1160 cm^{-1} and a little broad at 1490 cm^{-1} appear for C−H vibrations in the quinoid and semiquinone structure of PANI, reflecting the formation of PANI chains on the surfaces of GO in rGFP nanocomposites.

XRD studies of GO, rGF, and rGFP are shown in Figure 3d. In the spectra, a strong peak at 2θ = 11.2° appears for (002) plane of GO. The XRD patterns of rGF composites have exhibited peaks at 2θ = 30.3, 35.7, 43.3, 53.7 , 57.3, and 63° for the (220), (311), (400), (422), (333), and (440) planes of Fe_3O_4. The 002 plane of GO disappeared in the rGF, and these results suggest the in situ reduction of GO to rGO[24] and the formation of the Fe_3O_4 NPs on the rGO sheet.[38,39] After the polymerization of aniline to PANI, the peak position for Fe_3O_4 NPs of the rGF remains the same, along with a broad signature

DOI: 10.1021/acs.jpcc.6b10978
J. Phys. Chem. C 2017, 121, 7573−7583

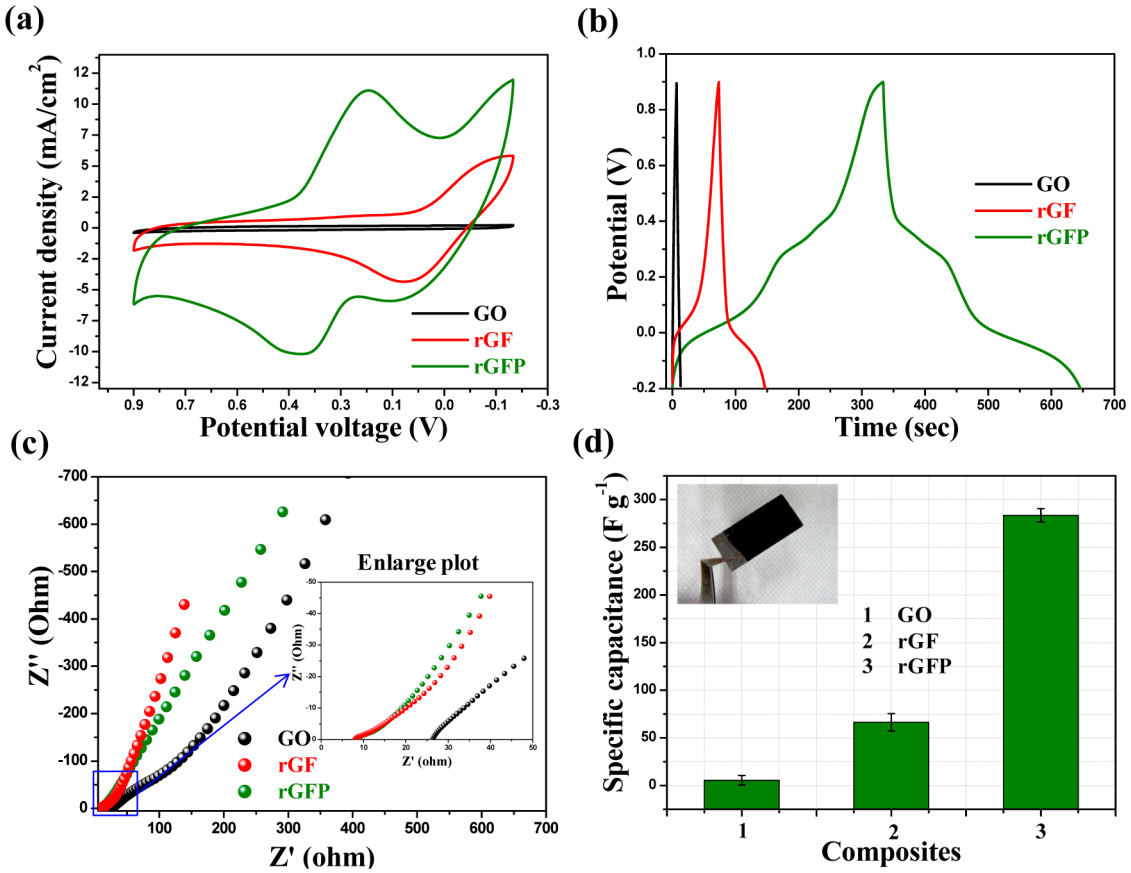

Figure 5. An all-solid-state electrochemical measurement for synthesized GO, rGF, and rGFP was carried out with the two-electrode method: (a) CV study at a scan speed of 50 mV/s, (b) GCD measurement at 1 A/g current density, (c) Nyquist plot of the rGFP composite-based flexible device in the 0.1 to 100 000 Hz frequency range, and (d) bar plot for specific capacitance with a different composite (inset digital image for a PANI-coated single electrode).

appearing at ∼25° that indicates the amorphous nature of PANI chains.[25]

The thermal stabilities of all synthesized composites have been measured in a TGA study (Figure 4a), and all materials have shown a mass loss of around 100 °C owing to the evaporation of adsorbed moisture on their surfaces. A sharp weight loss at 160−200 °C occurs for the decomposition of surface functional groups such as carboxylic acid, hydroxide, ketone, and epoxide.[40,41] Compared to GO, the thermal degradation of rGF in the 150−200 °C range is less owing to the presence of fewer oxygen-containing groups, and it indirectly supports the formation of rGO from GO by the in situ method. It is noted that rGFP shows a 31.4% thermal degradation (i.e., 68.6% retention) up to 550 °C. The weight loss of ∼220 °C is for the dedoping of rGO from the PANI main chain. The third weight loss starts at ∼490 °C because of the decomposition of PANI. It has been seen clearly that after 550 °C the temperature degradation values of GO, rGF, and rGFP composite are 55.7, 49.6, and 33.4%, respectively. Therefore, from the TGA study, it is concluded that rGFP nanocomposites have a higher thermal stability than do pristine GO and rGF.

The chemical composition and bonding nature of atoms for the synthesized rGFP composite are further characterized by XPS analysis. The peaks at ∼290, 404, 536, and 717 eV in wide-scan XPS spectra (Figure 4b) confirm the presence of C, N, O, and Fe, respectively.[41] The Fe_3O_4 nanoparticle formation is also revealed by the enlarged Fe 2p spectrum (Figure 4c), where peaks at 714.9 and 728 eV are characteristic of Fe $2p_{3/2}$ and Fe $2p_{1/2}$ of Fe_3O_4 nanoparticles.[42,43] The enlarged scans for N 1s (Figure 4d) of the rGFP composite were deconvoluted into three subpeaks at 401.5, 402.4, and 403.5 eV correspond to imine (−N═), amine (−NH−), and protonated amine ($-N^{+}-$) respectively.[16,26,44] The high-resolution C 1s spectrum has been deconvoluted into three subpeaks at 281.3, 283.2, and 283.8 eV for C═C/C−C, C−N/C−O, and C═O, respectively (Figure 4e), accompanying the formation of PANI.[16,26]

Electrochemical Measurement of an All-Solid-State Hybrid Supercapacitor. Recently, it has been demonstrated that the supercapacitor property of the polyaniline-based nanocomposite is modulated by the morphological change of the composite, and the presence of a nanorod in the composite has significantly influenced the enhancement of the capacitive performance of the composite as an electrode material. For practical applications of these materials, liquid electrolyte is replaced by the solid electrolyte to fabricate a thin all-solid-state supercapacitor device. The capacitive nature of synthesized composites has been measured by the classical two-electrode method.[17,19,29] The electrochemical performance of the prepared composite-modified electrode has been tested by CV, GCD, and EIS. For a comparison of the capacitive property of rGFP, two other devices have been prepared by synthesized GO and rGF composites. To prove the effect of Fe_3O_4-NPs on the electrochemical study, another similar device has been prepared on the basis of the synthesized rGO/PANI

DOI: 10.1021/acs.jpcc.6b10978
J. Phys. Chem. C 2017, 121, 7573−7583

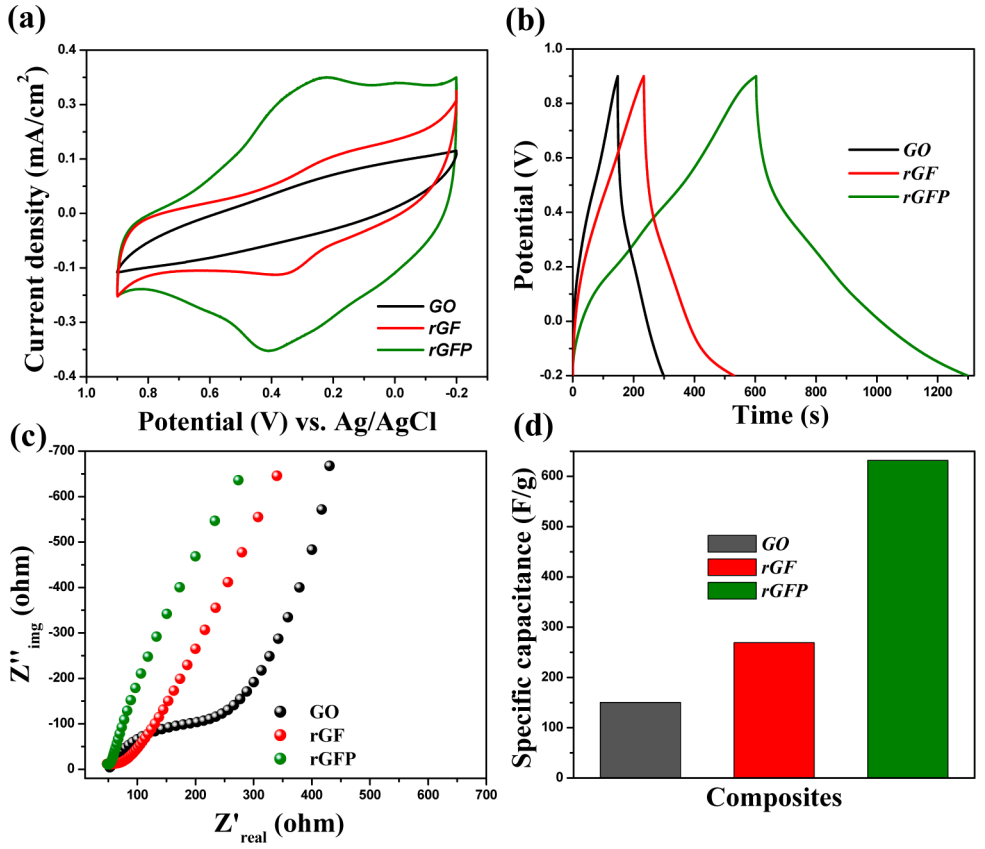

Figure 6. Electrochemical measurement (using the three-electrode system) of synthesized composites: (a) CV study (scan rate of 50 mV/s), (b) GCD study (at 1 A/g current density), (c) electrochemical impedance study (Nyquist plot, in the 0.1−100 000 Hz range), and (d) a bar plot for specific capacitance. All measurements were made in a 0.5 M H_3PO_4 aqueous solution.

composite using $FeCl_3$ as an oxidant, and its electrochemical behavior is shown in Figure S2.

Cyclic voltammetric studies of all synthesized composites have been recorded at a scan rate of 50 mV/s within the −0.2 to 0.9 V potential window (Figure 5a). The CV result clearly shows two oxidation peaks at 0.2 and −0.05 V for leucoemeraldine to emeraldine to pernigraniline as well as two reduction peaks at 0.1 and 0.37 V for pernigraniline to emeraldine to leucoemeraldine, revealing the formation of PANI in the rGFP nanocomposites. The energy storage capacity of any redox-active electrode material in the electrolyte is generally described by eq 4

$$q_t = q_{electrolyte} + q_{dl} + q_{electrode} \quad (4)$$

where q_t is the total charge stored in the electrode, $q_{electrolyte}$ is the charge stored due to the electrolyte (it is influential for the redox electrolyte), q_{dl} is charge stored due to the double-layer capacity, and q_{el} is the charge stored for the redox-active electrode material. If a measurement is carried out over the potential (ΔV), then $q_{electrode}/\Delta V$ should vary significantly with the applied potential because of the redox nature of the electrode material (Faradaic behavior). On the contrary, $q_{dl}/\Delta V$ should be independent of the applied potential because it is non-Faradaic in nature. It does mean that the CV of GO should be independent of the potential. However, in experiments the CV curve weakly depends on the potential because of the presence of a functional group at the edge of the GO surface. Unlike the double-layer capacitance in GO, both rGF and rGFP show dominant pseudocapacitance behavior that is required for the electrochemical performance of the hybrid supercapacitor devices. Current density and the area under the CV curve are higher for the rGFP composite than for GO and rGF, signifying the high charge-storage capacity of the rGFP nanorods.[16,29] The presence of both double-layer capacitance from graphene oxide and pseudocapacitance from polyaniline chains as well as Fe_3O_4 nanoparticles is significantly beneficial to realizing rGFP as a high-performance hybrid supercapacitor material.

The charge storage properties of the composites are further tested by the GCD method. Figure 5b illustrates the GCD study at 1 A/g current density of all synthesized GO, rGF, and rGFP composites. Unlike the conventional triangular shape of the GCD curve observed for GO only, a quasi-triangular shape of GCD curves is obtained for rGF and rGFP, confirming the presence of both the double-layer capacitance of GO and the pseudocapacitance of polyaniline chains as well as Fe_3O_4 nanoparticles. The longer charge−discharge time is overwhelmingly observed for the rGFP composite, and it supports the enhancement of the charge-storage property with the presence of PANI in the hybrid system. The specific capacitance (C_s) value has been calculated from the GCD curve using eq 1.[16,30,45]

Electrochemical impedance spectroscopic (EIS) studies of GO, rGF, and rGFP composites have been measured in the range of 0.1 to 100 kHz to evaluate the ability of different transport processes occurring in the composites. The high-frequency region, impedance spectrum generally depends on the charge-transport process, whereas the low-frequency region dominates the mass-transport process. The relative importance of the transport process solely depends on the steady-state

DOI: 10.1021/acs.jpcc.6b10978
J. Phys. Chem. C 2017, 121, 7573−7583

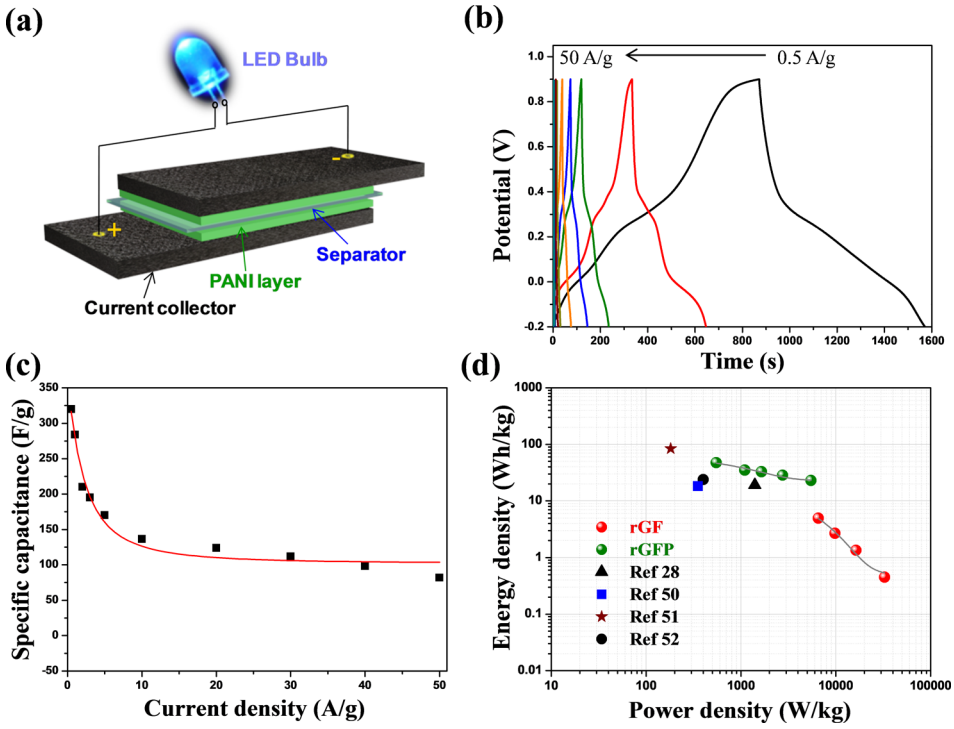

Figure 7. All flexible solid-state electrochemical study. (a) Model diagram for device making and LED lighting. (b) Galvanostatic charge−discharge measurement with different current densities. (c) Specific capacitance vs current density plot for the rGFP composite. (d) Ragone plot (energy density vs power density) of rGF and rGFP composites.

value of the potential at which the EIS measurement has been performed. The negligible semicircle response has been observed in the higher-frequency region for rGF and rGFP if results are presented in the Nyquist plot (Figure 5c), revealing the significantly low interfacial charge-transfer resistance. The high-frequency region indicates low (8.3 Ω) equivalent series resistance and also the 2.03 Ω charge-transfer resistance of composite materials.[29,48] The slope of the vertical line in the Nyquist plot in the low-frequency region is around ∼70°, indicating the nearly ideal capacitive behavior of the nanorods.[29,46,47,52] The calculated specific capacitance (C_s) values obtained for synthesized GO, rGF, and rGFP composites are 5.5, 66.4, and 283.4 F/g, respectively, through our design of the all-solid-state two-electrode sandwich system (Figure 5d).

Three-Electrode Electrochemical Performance of a Synthesized Composite. To compare the above results using a two-electrode system with a three-electrode system, a series of electrochemical experiments of three synthesized composites (GO, rGF, and rGFP) have been carried out (Figure 6) using the modified glassy carbon electrode (GCE) as a working electrode, a saturated calomel electrode (SCE) as the reference electrode, a Pt wire electrode as the counter electrode, and 0.5 M H_3PO_4 as a liquid electrolyte. As before, the CV results clearly demonstrate two oxidation peaks at 0.2 and −0.05 V for leucoemeraldine to emeraldine to pernigraniline as well as two reduction peaks at 0.1 and 0.37 V for pernigraniline to emeraldine to leucoemeraldine, revealing the formation of PANI in the rGFP nanocomposites (Figure 6a). Both rGF and rGFP revealing the dominantly pseudocapacitance behavior as compared to GO in the three-electrode system. The current density and the area under the CV curve are also higher for the rGFP composite than for GO and rGF, indicating the high charge storage capacity of rGFP. The quasi-triangular shape of the GCD curve has been observed for GO, rGF, and rGFP, confirming the presence of both the double-layer capacitance of GO and the pseudocapacitance of polyaniline chains as well as Fe_3O_4 nanoparticles. A longer charge−discharge time is also observed for the rGFP composite in three-electrode systems (Figure 6b). Impedance studies also reveal the negligible semicircle response observed in the higher-frequency region for rGF and rGFP as shown in the Nyquist plot (Figure 6c), indicating the low interfacial charge-transfer resistance. The estimated specific capacitance (C_s) values obtained for these composites using the three-electrode system are 136.9, 269.2, and 631.7 F/g, respectively (Figure 6d). It is worthwhile to note that the estimated value of the specific capacitance (C_s) of rGFP in the three-electrode system is 2 times higher than that of the two-electrode system.

The cartoon design of the symmetric all-solid-state supercapacitor device is shown in Figure 7a. The rGFP nanorod exhibits good capacitive behavior in CV within the scan speed ranging from 10 to 400 mV/s, and the working potential window is −0.2 to 0.9 V (Figure S1). GCD studies with various current densities (0.5 to 50 A/g) are illustrated in Figure 7b,c. The quasi-triangular shape of the charge−discharge curves, not perfectly straight lines, implies that faradic transformation occurs, and it confirms the pseudocapacitance behavior in the composite materials over the range of current densities.[48,49] To evaluate the performance of the rGFP composite for practical application, a Ragone plot is the best demonstration.[29,48] The energy density vs power density calculation for the symmetric device is plotted on the Ragone diagram (Figure 7d) from GCD curves. The maximum energy density that is achieved for our laboratory-made devices is 47.7 W h/kg at a power density of 550 W/kg for ternary rGFP nanocomposites. Obviously, the energy density delivered by the rGFP composite is higher than that of the rGF nanocomposite because part of the pseudocapacitance from the PANI nanorod is contributing to

DOI: 10.1021/acs.jpcc.6b10978
J. Phys. Chem. C 2017, 121, 7573−7583

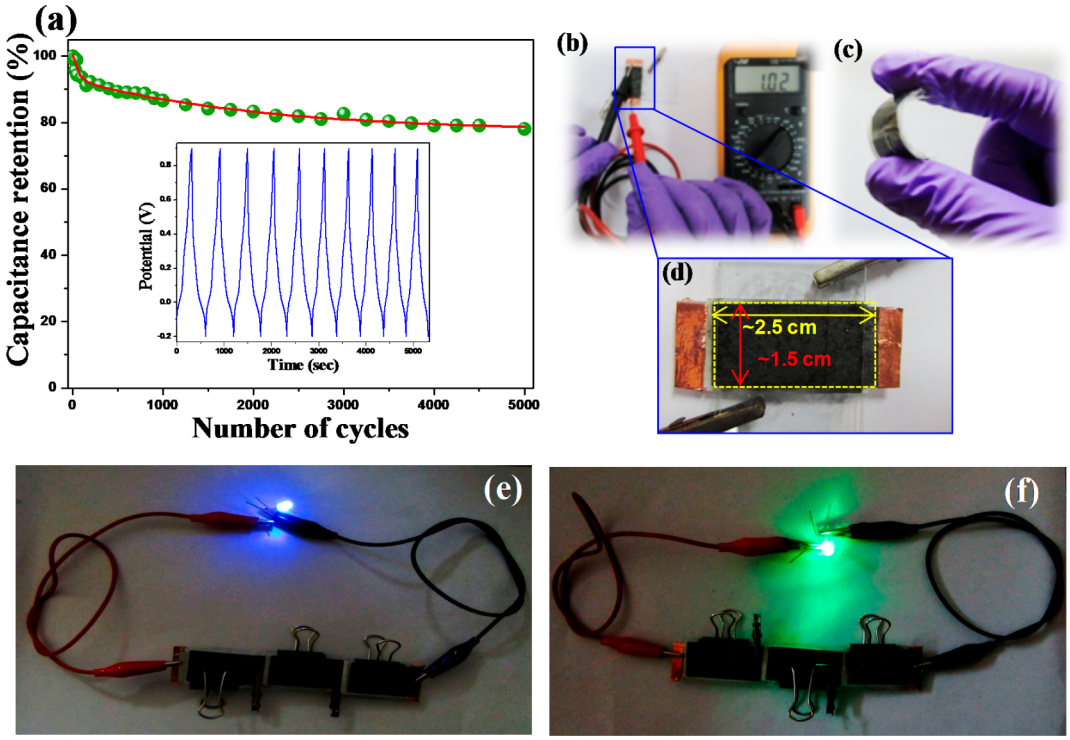

Figure 8. (a) Five thousand charge−discharge cyclic lifetime measurements (inset curve for 10 consecutive GCD cycles). (b, c) Photograph for handmade thin supercapacitor devices showing ∼1.02 V. (d) Dimensions of a single device. (e, f) Blue and green LEDs glowing via handmade supercapacitor devices.

the total capacitance. The power density and energy density of our design device are better than for some previously symmetrical devices.[28,50−52] A fabricated all-solid-state supercapacitor device based on the rGFP composite shows little mechanical strength at 9.2 MPa, and the elongation due to breakage is 4.2 MPa (Figure S5).

The long-term lifecycle stability of the prepared composite device has been tested for up to 5000 cycles through a repeated charge−discharge process at 1 A/g current density (Figure 8a). After 5000 cycles, ∼78% property retention occurs, proving the excellent long-term cycling stability of rGF materials. The making of all solid-state devices that avoids the weight loss of active materials during the repeated charge−discharge process, as a result of long-term stability, has been achieved. Furthermore, the voltage has been monitored by a multimeter (roughly) for a single device having dimensions of 2.5 cm × 1.5 cm, and it is ∼1.02 V each (Figure 8b−d).

Finally, we have demonstrated LED bulb (operating voltage, ∼1.5 V) lighting for real applications (Figure 8e,f) by connecting three such devices in a series (where each device provided ∼1.02 V). After the device was charged, the LED glowed very well for about 30 min, showing the impressive application of our solid-state supercapacitor devices (Supporting Information video).

CONCLUSIONS

We have synthesized an rGO/Fe_3O_4/PANI nanocomposite by a soft-template-based method that is characterized with the help of UV−vis, IR, SEM, TEM, XPS, XRD, and Raman studies. Subsequently, these composites are utilized to fabricate all-solid-state semiflexible and binder-free supercapacitor devices. The thin supercapacitor device shows excellent electrochemical energy storage performance such as a high specific capacity, high energy density, high power density, and excellent cycling stability (78% retention after the 5000th cycle). The double-layer capacitance from rGO and the pseudocapacitance from Fe_3O_4 nanoparticles and PANI nanords jointly assist to improve the high-performance all-solid-state hybrid charge storage properties. Moreover, for practical application we demonstrate LED light illumination using our design supercapacitor device based on synthesized rGO/Fe_3O_4/PANI materials and its glow for up to 30 min. Thus, the nanorods have the potential to make significant flexible and portable supercapacitors via energy storage technology.

ASSOCIATED CONTENT

Supporting Information

The Supporting Information is available free of charge on the ACS Publications website at DOI: 10.1021/acs.jpcc.6b10978.

Synthesis of GO, preparation of composites, previous work report, CV curve with various scan speeds, a stress−strain curve, BET results, and optimization of the potential window (PDF)

Supporting video (AVI)

AUTHOR INFORMATION

Corresponding Author

*E-mail: psusm2@iacs.res.in.

ORCID

Sudip Malik: 0000-0001-5358-5653

Notes

The authors declare no competing financial interest.

DOI: 10.1021/acs.jpcc.6b10978
J. Phys. Chem. C 2017, 121, 7573−7583

■ ACKNOWLEDGMENTS

S. Malik acknowledges CSIR, India (project no. 02(0161)/13/EMR-II) for financial support. S. Mondal is indebted to CSIR, New Delhi, India for his fellowship. We are thankful to the Unit of Nanoscience (DST, Government of India) at IACS, Kolkata, for XPS.

■ REFERENCES

(1) Simon, P.; Gogotsi, Y. Materials for Electrochemical Capacitors. *Nat. Mater.* **2008**, *7*, 845−854.
(2) Yang, Z.; Zhang, J.; Kintner-Meyer, M. C.; Lu, X.; Choi, D.; Lemmon, J. P.; Liu, J. Electrochemical Energy Storage for Green Grid. *Chem. Rev.* **2011**, *111*, 3577−3613.
(3) Nishide, H.; Oyaizu, K. Materials Science Toward Flexible Batteries. *Science* **2008**, *319*, 737−738.
(4) Winter, M.; Brodd, R. J. What Are Batteries, Fuel Cells, and Supercapacitors? *Chem. Rev.* **2004**, *104*, 4245−4270.
(5) El-Kady, M. F.; Kaner, R. B. Scalable Fabrication of High-Power Graphene Micro-Supercapacitors for Flexible and On-Chip Energy Storage. *Nat. Commun.* **2013**, *4*, 1475.
(6) Wang, G.; Zhang, L.; Zhang, J. A Review of Electrode Materials for Electrochemical Supercapacitors. *Chem. Soc. Rev.* **2012**, *41*, 797−828.
(7) Huang, L.; Li, C.; Shi, G. High-Performance and Flexible Electrochemical Capacitors Based on Graphene/Polymer Composite Films. *J. Mater. Chem. A* **2014**, *2*, 968−974.
(8) Zhang, L. L.; Zhao, X. Carbon Based Materials as Supercapacitor Electrodes. *Chem. Soc. Rev.* **2009**, *38*, 2520−2531.
(9) Lu, X.; Zhai, T.; Zhang, X.; Shen, Y.; Yuan, L.; Hu, B.; Gong, L.; Chen, J.; Gao, Y.; Zhou, J. WO_{3-X}@Au@MnO_2 Core-Shell Nanowires on Carbon Fabric for High-Performance Flexible Supercapacitors. *Adv. Mater.* **2012**, *24*, 938−944.
(10) Jiang, J.; Li, Y.; Liu, J.; Huang, X.; Yuan, C.; Lou, X. W. D. Recent Advances in Metal Oxide Based Electrode Architecture Design for Electrochemical Energy Storage. *Adv. Mater.* **2012**, *24*, 5166−5180.
(11) Pendashteh, A.; Rahmanifar, M. S.; Kaner, R. B.; Mousavi, M. F. Facile Synthesis of Nanostructured $CuCo_2O_4$ as a Novel Electrode Material for High-Rate Supercapacitors. *Chem. Commun.* **2014**, *50*, 1972−1975.
(12) Zhang, L. L.; Zhao, X. Carbon Based Materials as Supercapacitor Electrodes. *Chem. Soc. Rev.* **2009**, *38*, 2520−2531.
(13) Zang, X.; Li, X.; Zhu, M.; Li, X.; Zhen, Z.; He, Y.; Wang, K.; Wei, J.; Kang, F.; Zhu, H. Graphene/Polyaniline Woven Fabric Composite Films as Flexible Supercapacitor Electrodes. *Nanoscale* **2015**, *7*, 7318−7322.
(14) Wang, L.; Lu, X.; Lei, S.; Song, Y. Graphene-Based Polyaniline Nanocomposites: Preparation, Properties and Applications. *J. Mater. Chem. A* **2014**, *2*, 4491−4509.
(15) Cai, G.; Darmawan, P.; Cui, M.; Wang, J.; Chen, J.; Magdassi, S.; Lee, P. S. Highly Stable Transparent Conductive Silver Grid/PEDOT:PSS Electrodes for Integrated Bifunctional Flexible Electrochromic Supercapacitors. *Adv. Energy Mater.* **2016**, *6*, 1501882.
(16) Mondal, S.; Rana, U.; Malik, S. Graphene Quantum Dot-Doped Polyaniline Nanofiber as High Performance Supercapacitor Electrode Materials. *Chem. Commun.* **2015**, *51*, 12365−12368.
(17) Lu, X.; Yu, M.; Wang, G.; Tong, Y.; Li, Y. Flexible Solid-State Supercapacitors: Design, Fabrication and Applications. *Energy Environ. Sci.* **2014**, *7*, 2160−2181.
(18) Kurra, N.; Hota, M. K.; Alshareef, H. N. Conducting Polymer Micro-Supercapacitors for Flexible Energy Storage and Ac Line-Filtering. *Nano Energy* **2015**, *13*, 500−508.
(19) Weng, Z.; Su, Y.; Wang, D. W.; Li, F.; Du, J.; Cheng, H. M. Graphene-Cellulose Paper Flexible Supercapacitors. *Adv. Energy Mater.* **2011**, *1*, 917−922.
(20) Zeng, S.; Chen, H.; Cai, F.; Kang, Y.; Chen, M.; Li, Q. Electrochemical Fabrication of Carbon Nanotube/Polyaniline Hydrogel Film for All-Solid-State Flexible Supercapacitor with High Areal Capacitance. *J. Mater. Chem. A* **2015**, *3*, 23864−23870.
(21) Yang, X.; Zhang, F.; Zhang, L.; Huang, Y.; Chen, Y. A High Performance Graphene Oxide Doped Ion Gel as Gel Polymer Electrolyte for All-Solid-State Supercapacitor Applications. *Adv. Funct. Mater.* **2013**, *23*, 3353−3360.
(22) Nithya, V. D.; Arul, N. S. Progress and Development of Fe_3O_4 Electrodes for Supercapacitors. *J. Mater. Chem. A* **2016**, *4*, 10767−10778.
(23) Shao, Y.; El-Kady, M. F.; Wang, L. J.; Zhang, Q.; Li, Y.; Wang, H.; Mousavi, M. F.; Kaner, R. B. Graphene-Based Materials for Flexible Supercapacitors. *Chem. Soc. Rev.* **2015**, *44*, 3639−3665.
(24) Rana, U.; Malik, S. Graphene Oxide/Polyaniline Nanostructures: Transformation of 2D Sheet to 1D Nanotube and *in-situ* Reduction. *Chem. Commun.* **2012**, *48*, 10862−10864.
(25) Rana, U.; Chakrabarti, K.; Malik, S. Benzene Tetracarboxylic Acid Doped Polyaniline Nanostructures: Morphological, Spectroscopic and Electrical Characterization. *J. Mater. Chem.* **2012**, *22*, 15665−15671.
(26) Mondal, S.; Rana, U.; Malik, S. Facile Decoration of Polyaniline Fiber with Ag Nanoparticles for Recyclable SERS Substrate. *ACS Appl. Mater. Interfaces* **2015**, *7*, 10457−10465.
(27) Wang, K.; Wu, H.; Meng, Y.; Wei, Z. Conducting Polymer Nanowire Arrays for High Performance Supercapacitors. *Small* **2014**, *10*, 14−31.
(28) Wu, Q.; Xu, Y.; Yao, Z.; Liu, A.; Shi, G. Supercapacitors Based on Flexible Graphene/Polyaniline Nanofiber Composite Films. *ACS Nano* **2010**, *4*, 1963−1970.
(29) Anothumakkool, B.; Torris, A. T. A.; Bhange, S. N.; Unni, S. M.; Badiger, M. V.; Kurungot, S. Design of a High Performance Thin All-Solid-State Supercapacitor Mimicking the Active Interface of Its Liquid-State Counterpart. *ACS Appl. Mater. Interfaces* **2013**, *5*, 13397−13404.
(30) Xie, Y.; Liu, Y.; Zhao, Y.; Tsang, Y. H.; Lau, S. P.; Huang, H.; Chai, Y. Stretchable All-Solid-State Supercapacitor with Wavy Shaped Polyaniline/Graphene Electrode. *J. Mater. Chem. A* **2014**, *2*, 9142−9149.
(31) Zeng, H.; Li, J.; Wang, Z.; Liu, J.; Sun, S. Bimagnetic Core/Shell FePt/Fe_3O_4 Nanoparticles. *Nano Lett.* **2004**, *4*, 187−190.
(32) Zhang, Y.; Ma, H.-L.; Zhang, Q.; Peng, J.; Li, J.; Zhai, M.; Yu, Z.-Z. Facile Synthesis of Well-Dispersed Graphene by γ-Ray Induced Reduction of Graphene Oxide. *J. Mater. Chem.* **2012**, *22*, 13064−13069.
(33) Yang, S.; Yue, W.; Huang, D.; Chen, C.; Lin, H.; Yang, X. A Facile Green Strategy for Rapid Reduction of Graphene Oxide by Metallic Zinc. *RSC Adv.* **2012**, *2*, 8827−8832.
(34) Paredes, J.; Villar-Rodil, S.; Martinez-Alonso, A.; Tascon, J. Graphene Oxide Dispersions in Organic Solvents. *Langmuir* **2008**, *24*, 10560−10564.
(35) Zhao, X.; Zhang, Q.; Chen, D.; Lu, P. Enhanced Mechanical Properties of Graphene-Based Poly (Vinyl Alcohol) Composites. *Macromolecules* **2010**, *43*, 2357−2363.
(36) Li, X. G.; Li, A.; Huang, M. R. Facile High-Yield Synthesis of Polyaniline Nanosticks with Intrinsic Stability and Electrical Conductivity. *Chem. - Eur. J.* **2008**, *14*, 10309−10317.
(37) Deore, B. A.; Yu, I.; Freund, M. S. A Switchable Self-Doped Polyaniline: Interconversion Between Self-Doped and Non-Self-Doped Forms. *J. Am. Chem. Soc.* **2004**, *126*, 52−53.
(38) Li, H.; Liao, J.; Xibin, Z. Facile Synthesis of Single Crystal Fe_3O_4 Sub-Microcubes Free of Any Capping Agent and Their Catalytic Performance in *p*-Nitrophenol Reduction. *J. Mater. Chem. A* **2014**, *2*, 17530−17535.
(39) Li, L.; Dou, Y.; Wang, L.; Luo, M.; Liang, J. One-Step Synthesis of High-Quality N-Doped Graphene/Fe_3O_4 Hybrid Nanocomposite and Its Improved Supercapacitor Performances. *RSC Adv.* **2014**, *4*, 25658−25665.
(40) McAllister, M. J.; Li, J.-L.; Adamson, D. H.; Schniepp, H. C.; Abdala, A. A.; Liu, J.; Herrera-Alonso, M.; Milius, D. L.; Car, R.; Prud'homme, R. K. Single Sheet Functionalized Graphene by Oxidation and Thermal Expansion of Graphite. *Chem. Mater.* **2007**, *19*, 4396−4404.

DOI: 10.1021/acs.jpcc.6b10978
J. Phys. Chem. C 2017, 121, 7573−7583

(41) Kuila, T.; Mishra, A. K.; Khanra, P.; Kim, N. H.; Uddin, M. E.; Lee, J. H. Facile Method for the Preparation of Water Dispersible Graphene Using Sulfonated Poly (Ether−Ether−Ketone) and Its Application as Energy Storage Materials. *Langmuir* **2012**, *28*, 9825−9833.
(42) Ji, L.; Zhou, L.; Bai, X.; Shao, Y.; Zhao, G.; Qu, Y.; Wang, C.; Li, Y. Facile Synthesis of Multiwall Carbon Nanotubes/Iron Oxides for Removal of Tetrabromobisphenol A and Pb(II). *J. Mater. Chem.* **2012**, *22*, 15853−15862.
(43) Zhu, C.-L.; Zhang, M.-L.; Qiao, Y.-J.; Xiao, G.; Zhang, F.; Chen, Y.-J. Fe_3O_4/TiO_2 Core/Shell Nanotubes: Synthesis and Magnetic and Electromagnetic Wave Absorption Characteristics. *J. Phys. Chem. C* **2010**, *114*, 16229−16235.
(44) Li, Y.; Zhao, X.; Yu, P.; Zhang, Q. Oriented Arrays of Polyaniline Nanorods Grown on Graphite Nanosheets for an Electrochemical Supercapacitor. *Langmuir* **2013**, *29*, 493−500.
(45) Ghosh, D.; Giri, S.; Das, C. K. Synthesis, Characterization and Electrochemical Performance of Graphene Decorated with 1D $NiMoO_4{\cdot}nH_2O$ Nanorods. *Nanoscale* **2013**, *5*, 10428−10437.
(46) Zhou, W.; Liu, X.; Sang, Y.; Zhao, Z.; Zhou, K.; Liu, H.; Chen, S. Enhanced Performance of Layered Titanate Nanowire Based Supercapacitor Electrodes by Nickel Ion Exchange. *ACS Appl. Mater. Interfaces* **2014**, *6*, 4578−4586.
(47) Zhu, S.; Wu, M.; Ge, M.-H.; Zhang, H.; Li, S.-K.; Li, C.-H. Design and Construction of Three-Dimensional CuO/Polyaniline/rGO Ternary Hierarchical Architectures for High Performance Supercapacitors. *J. Power Sources* **2016**, *306*, 593−601.
(48) Chen, W.; Rakhi, R.; Alshareef, H. N. Facile Synthesis of Polyaniline Nanotubes Using Reactive Oxide Templates for High Energy Density Pseudocapacitors. *J. Mater. Chem. A* **2013**, *1*, 3315−3324.
(49) Zeng, S.; Chen, H.; Cai, F.; Kang, Y.; Chen, M.; Li, Q. Electrochemical Fabrication of Carbon Nanotube/Polyaniline Hydrogel Film for All-Solid-State Flexible Supercapacitor with High Areal Capacitance. *J. Mater. Chem. A* **2015**, *3*, 23864−23870.
(50) Fan, H.; Niu, R.; Duan, J.; Liu, W.; Shen, W. Fe_3O_4@Carbon Nanosheets for All-Solid-State Supercapacitor Electrodes. *ACS Appl. Mater. Interfaces* **2016**, *8*, 19475−19483.
(51) Chen, W.; Rakhi, R.; Alshareef, H. N. Facile Synthesis of Polyaniline Nanotubes Using Reactive Oxide Templates for High Energy Density Pseudocapacitors. *J. Mater. Chem. A* **2013**, *1*, 3315−3324.
(52) Chi, K.; Zhang, Z.; Xi, J.; Huang, Y.; Xiao, F.; Wang, S.; Liu, Y. Freestanding Graphene Paper Supported Three-Dimensional Porous Graphene−Polyaniline Nanocomposite Synthesized by Inkjet Printing and in Flexible All-Solid-State Supercapacitor. *ACS Appl. Mater. Interfaces* **2014**, *6*, 16312−16319.

DOI: 10.1021/acs.jpcc.6b10978
J. Phys. Chem. C 2017, 121, 7573−7583